

Investigations of key issues on the reproducibility of high- T_c superconductivity emerging from compressed $\text{La}_3\text{Ni}_2\text{O}_7$

Yazhou Zhou^{1*}, Jing Guo^{1*}, Shu Cai^{2*}, Hualei Sun^{3*}, Pengyu Wang^{1,4}, Jinyu Zhao^{1,4},
Jinyu Han^{1,4}, Xintian Chen^{1,4}, Yongjin Chen², Qi Wu¹, Yang Ding²,
Tao Xiang^{1,4,5}, Ho-kwang Mao^{2†} and Liling Sun^{1,2,4†}

¹*Institute of Physics, Chinese Academy of Sciences, Beijing 100190, China*

²*Center for High Pressure Science & Technology Advanced Research, Beijing 100094, China*

³*School of Science, Sun Yat-Sen University, Shenzhen, Guangdong 518107, China*

⁴*University of Chinese Academy of Sciences, Beijing 100190, China*

⁵*Beijing Academy of Quantum Information Sciences, Beijing 100193, China*

Recently, the signatures of superconductivity near 80 K have been discovered in the single crystal of $\text{La}_3\text{Ni}_2\text{O}_7$ under pressure¹, which makes it a new candidate of the high-temperature superconductors dominated by $3d$ transition elements after the cuprate and iron-pnictide superconductors²⁻⁴, and thus has attracted significant attention. However, there are several critical issues that have been perplexing the scientific community. These include (1) what factors contribute to the poor reproducibility of the experimental results, (2) what the intrinsic nature of the pressure-induced superconductivity is, bulk or filamentary, (3) where the superconducting phase locates within the sample if it is indeed filamentary, and (4) what the oxygen content is necessary for the development and stabilization of superconductivity. In this study, we employ comprehensive high-pressure measurements to address these crucial issues. By demonstrating both zero resistance and diamagnetism, we are the first to confirm the existence of high-temperature superconductivity in $\text{La}_3\text{Ni}_2\text{O}_7$. Through our sensitive *ac* susceptibility measurements, we are the first to quantify the superconducting volume fraction in $\text{La}_3\text{Ni}_2\text{O}_7$ at the level of 1%. In tandem with our observation of the anisotropic zero-resistance state only in some of the samples, we suggest that the superconductivity in this nickelate is filamentary-like. By our scanning transmission electron microscopy (STEM) investigations, we propose that the filamentary superconductivity most likely emerges at the interface between the $\text{La}_3\text{Ni}_2\text{O}_7$ and $\text{La}_4\text{Ni}_3\text{O}_{10}$ phases. Further, the upper and lower bounds of the oxygen content required for the presence of superconductivity were determined to be 7.35 and 6.89, respectively. Our results provide not only new insights into understanding the puzzling issues in this material, but also significant information for achieving a better understanding on the superconductivity of this material.

The quest for novel high-temperature superconductors is motivated by the expectation that these materials could have practical applications or lead to a better understanding of the fundamental mechanisms underlying high-temperature superconductivity. A possible fruitful area predicted to investigate is the nickelates⁵. Several candidates for superconductivity have been found in the thin-film nickelates⁶⁻¹⁰. Recently, the signatures of superconductivity with a transition temperature (T_c) near 80 K have been discovered in the single crystal $\text{La}_3\text{Ni}_2\text{O}_7$ under high pressure³. This high- T_c compound has garnered considerable interest in the past months, and a great deal of advancements have been achieved primarily by theorists¹¹⁻³⁹. The results from the high-resolution angle-resolved photoemission spectroscopy⁴⁰⁻⁴² suggest that the ambient-pressure $\text{La}_3\text{Ni}_2\text{O}_7$ exhibits a strong correlation characteristic⁴³ associated with the covalent hybridization between transition metal $3d$ and O $2p$ orbitals, which is similar to the formation of the Zhang-Rice singlet in cuprates^{33,44}. These observations suggest that $\text{La}_3\text{Ni}_2\text{O}_7$ holds the potential to exhibit intriguing phenomena under specific non-thermal control parameters, such as pressure.

On the experimental side, although zero resistance has been observed in some compressed nickelate samples^{45,46}, most of them cut even from the same batch show no zero resistance superconductivity. The anomalously irreproducible superconductivity suggests the possibility of an inhomogeneous distribution of a small amount of the superconducting phase within the crystal. In addition, the signature of the high- T_c superconductivity was also observed in the $\text{La}_3\text{Ni}_2\text{O}_7$ polycrystalline samples, but no Meissner effect was reported in these papers^{29,47,48}. Recent experimental results

regarding the characterization of the $\text{La}_3\text{Ni}_2\text{O}_7$ single crystals have revealed the existence of minor intergrowth phases within the majority phase that exhibits a stacking sequence composed of bilayer and bilayer blocks with alternating NiO_6 octahedra (referred to as 2222 or 327 phase). These intergrowth phases include the 214 phase characterized by single layer blocks, the 4310 phase characterized by trilayer blocks, and a polymorphic phase featuring both single and trilayer blocks (referred to as 22221313)⁴⁹⁻⁵³. These results suggest that this material may exhibit a more complex physics associated with high- T_c superconductivity compared to the pure 327 phase, which needs a comprehensive investigation.

In this study, we conducted the first high-pressure measurements on the superconducting volume fraction of the compressed $\text{La}_3\text{Ni}_2\text{O}_7$ using a modulated alternating-current (*ac*) susceptibility system. The employed system possesses the ability to detect a superconducting volume fraction as low as 0.5% (the details can be found in Supplementary Information - SI). Moreover, we performed *in-situ* resistance, Hall coefficient and scanning transmission electron microscopy (STEM) investigations, with the attempt to elucidate the underlying cause of the anomalous superconductivity observed in the compressed $\text{La}_3\text{Ni}_2\text{O}_7$.

Before conducting the high-pressure experiments, we performed structural characterization and resistance measurements on the single crystal $\text{La}_3\text{Ni}_2\text{O}_7$ sample at ambient pressure (see SI). The single crystal X-ray diffraction reveals that the structure of our sample crystallizes in an orthorhombic unit cell in the *Amam* space, in good agreement with the results reported in Ref. [3]. The temperature dependence of

resistance for the ambient-pressure sample shows a metallic behavior upon cooling, consistent with the reported results³. In the high-pressure modulated *ac* susceptibility measurements, we loaded a piece of elemental vanadium, with the nearly half volume of the La₃Ni₂O₇ sample, in the same high-pressure chamber as a reference to determine the superconducting volume fraction of the La₃Ni₂O₇ sample. By comparing their diamagnetic signal magnitude, after accounting for the influence of their demagnetizing factor (see SI), we were able to estimate the superconducting volume fraction of the La₃Ni₂O₇ sample and the pressure applied on the sample through the pressure-dependent T_c of the vanadium⁵⁴. Figure 1 shows the temperature dependence of the modulated *ac* susceptibility ($\Delta\chi'$) obtained at different pressures. Below 20.7 GPa, no superconducting transition is observed, and only the background signal is detected (Fig. 1a-1c). While, in this pressure range, the superconducting transitions of the elemental vanadium can be clearly identified by a sudden increase in the signal above the background (the arrow indicates the onset temperature of the superconducting transition, see the insets of Fig. 1a-1c). Upon increasing the pressure to 22 GPa, a ‘broad-peak’ emerges at 64.3 K (Fig. 1d). According to the theory of the modulated magnetic susceptibility⁵⁵⁻⁵⁷, this ‘peak’ results from the superconducting transition of the sample, instead of a magnetic transition (see SI). To enhance the visibility, we mark the broad peak in light green with the background represented by a dashed line. This kind of broad peak can be observed up to 28.2 GPa, the highest pressure investigated in this run (Fig. 1d-1f).

We calculated the superconducting volume fraction of the La₃Ni₂O₇ single crystal

samples by comparing the results obtained from the reference sample of vanadium. Assuming the superconducting volume fraction of vanadium is 100%, we find that the superconducting volume fraction of $\text{La}_3\text{Ni}_2\text{O}_7$ is approximately $\sim 1.0\%$ at 22.0 GPa (see SI).

Furthermore, we found that the superconducting transition temperature slightly decreases with increasing pressure, as shown in Fig. 1d-1f, consistent with the resistance measurements reported in the previous studies^{3,45,46}. Then, we released the pressure starting from 28.2 GPa and found a slight increase in T_c (Fig. 1g-1h), in which the maximum T_c reached 65.2 K at 21.2 GPa. As the pressure was further released to 17.2 GPa, the superconducting diamagnetic signal became invisible, consistent with the behavior where the pressure was increased to the same level (Fig. 1b and 1c). This indicates that the pressure-induced transition is reversible. However, unexpectedly, in our five independent measurements on the samples cut from the same batch, we observed the superconducting diamagnetic transition only once (see SI). In addition, we also did the *ac* susceptibility measurement on the $\text{La}_3\text{Ni}_2\text{O}_7$ single crystal sample using a non-modulated *ac* susceptibility system (the sample signal is detected by a single-phase-locked amplifier), the approach same as that used in Ref. [3], and did not observe any evidence of superconducting diamagnetic transition (see SI).

Next, we performed high-pressure resistance measurements on the $\text{La}_3\text{Ni}_2\text{O}_7$ single crystal samples. We have measured seven samples, but observed the presence of superconductivity with zero resistance only in one of them. Figure 2 shows the results from two of the samples (A and B). Sample A displays a semiconducting-like behavior

at the pressure below 7.9 GPa. Its resistance starts to drop at the low temperature at 11.1 GPa (Fig. 2a). This drop becomes more pronounced with increasing pressure. It approaches zero above 21.5 GPa (Fig. 2b). For sample B, zero resistance is observed when the pressure is applied between 17.8 GPa and 31.5 GPa (see the inset of Fig. 2c), which confirms the occurrence of superconducting transition in $\text{La}_3\text{Ni}_2\text{O}_7$. Subsequently, we released the pressure from 31.5 GPa down to 5.5 GPa, and observed a gradual loss of superconductivity (Fig. 2d), consistent with our findings from the modulated ac susceptibility measurements (Fig. 1). At 5.5 GPa, the sample returns to its semiconducting phase (Fig. 2d), indicating that the pressure-induced transition from the semiconducting state to the superconducting state is reversible.

Figure 3 shows the phase diagram obtained based on our ac susceptibility and transport measurements for $\text{La}_3\text{Ni}_2\text{O}_7$. In this diagram, we have also included the density-wave-like (DW-like) phase transition temperature (T_D) reported in Ref. [43] and the T_c s reported by other groups^{3,45,46}. It is shown that the application of pressure suppresses the DW-like phase⁴³ and then induces a superconducting (SC) transition at a critical pressure (P_c) above 10 GPa (Fig.3a).

In addition, we conducted Hall measurements on the sample (see SI) and found that the Hall coefficient R_H remains positive across the investigated pressure range with a notable drop at around P_c (Fig.3b). This positive Hall coefficient and the sudden change align with the trends observed in the studies on the Sr-doped LaNiO_2 ⁷. Since the sample undergoes a structure phase transition from an ambient-pressure orthorhombic $Amam$ phase to a high-pressure orthorhombic $Fmmm$ phase at the

temperature of our Hall measurements^{3,58}, the drop in R_H at the boundary between the DW-like and the normal state of the superconducting (SC) phases suggests that the pressure-induced structure phase transition alters the electronic structure of the material.

The observation of the maximum superconducting volume fraction at the level of $\sim 1\%$ and the fact that it is difficult to obtain a zero-resistance state suggest that the superconductivity in $\text{La}_3\text{Ni}_2\text{O}_7$ is likely filamentary in nature⁵⁹⁻⁶¹. This speculation accounts for several enigmas regarding the pressure-induced superconductivity in the $\text{La}_3\text{Ni}_2\text{O}_7$ single crystal sample. As an example, when conducting resistance measurements along different directions of the sample, we found that zero resistance was observed in only one direction while not in the other, despite having the same onset T_c values in both directions (see SI).

In order to provide more evidence for the proposed filamentary superconductivity in compressed $\text{La}_3\text{Ni}_2\text{O}_7$, we performed high-pressure resistance measurements on the sample using various current values (ranging from 0.01 mA to 1 mA). We found a non-Ohmic behavior below T_c and non-linear V - I characteristic (see SI), supporting that the superconductivity in $\text{La}_3\text{Ni}_2\text{O}_7$ is filamentary.

Similar to what has been observed in cuprate superconductors^{1,2,62,63} the deviation from stoichiometric oxygen content in $\text{La}_3\text{Ni}_2\text{O}_7$ appears to have a significant impact on the presence of superconductivity⁶⁴. To establish the connection of the oxygen content in $\text{La}_3\text{Ni}_2\text{O}_7$ with the presence of superconductivity, we performed the comprehensive investigations starting with the synthesis of polycrystalline samples by using sol-gel method (see SI). The characterization on the as-grown samples found that

they can be well indexed by the orthorhombic structure in the *Amam* space group (see SI), which is consistent with the structure of the single crystal sample reported in Ref. [3]. The oxygen content of the as-grown sample was estimated to be about 6.88 determined by thermalgravimetric analysis (see SI). Subsequently, we adjusted the oxygen content over a wide range using the electrochemical method^{63,65,66} (see SI), and conducted combined measurements of resistance and modulated *ac* susceptibility on the same sample in a diamond anvil cell. As shown in Fig. 4a, the superconductivity was observed only within a specific range of the oxygen content, ranging from 6.88 ($\delta = -0.12$) to 7.42 ($\delta = 0.42$). Intriguingly, within this range, the maximum T_c value remains nearly unchanged, which suggests that, when the oxygen content falls in an appropriate range, it no longer significantly affects the maximum T_c value. Based on these results, we determined the upper and lower bounds of the oxygen content required for the development of superconductivity to be about 7.35 and 6.89, respectively. Outside this range, superconductivity was no longer observed.

Remarkably, we noticed that there exists a distinct narrow range of oxygen content inside the superconducting regime (see the shaded area in Fig. 4a). Within this regime, the oxygen content in $\text{La}_3\text{Ni}_2\text{O}_7$ closely approaches 7, and the corresponding normal-state resistance of the sample exhibits a metallic behavior. Differently, outside this regime the normal-state resistance demonstrates a semiconducting-like behavior and displays a prominent upturn at low temperature. These observations indicate the crucial role of the stoichiometric oxygen content on the metallization and the emergence of superconductivity in this material.

The modulated *ac* susceptibility measurements were also conducted on the same polycrystalline samples that we investigated for the resistance measurements. Not surprisingly, we did not observe any superconducting diamagnetic signal in the samples with oxygen contents ranging from 6.88 to 7.42 (see Fig. 4a-(1) to Fig. 4a-(4)). As a result, we propose that the superconducting volume fraction in these polycrystalline samples should be less than 0.5%, which is the detectable limit of our measuring system (see SI). These findings suggest that the superconductivity in $\text{La}_3\text{Ni}_2\text{O}_7$ is unlikely to exist on the surface of the crystal, because the enhanced specific surface area of the polycrystalline sample does not increase the superconducting volume fraction.

To further understand the perplexing superconducting behavior of $\text{La}_3\text{Ni}_2\text{O}_7$, we performed STEM investigations on the single crystal and polycrystalline samples (Fig. 4b-4d). Based on our results, we found that the predominant phase (>95%) is the $\text{La}_3\text{Ni}_2\text{O}_7$ (327) phase with the 2222-stacking sequence, and the minor phases (< 5%) are the $\text{La}_4\text{Ni}_3\text{O}_{10}$ (4310) and $\text{La}_2\text{Ni}_1\text{O}_4$ (214) phases. Based on these observations, we engage in the following discussions to address various perplexing issues:

(1) Despite the dominating phase of the single crystal sample is the 327 phase, the 327 phase itself should not be responsible for the superconductivity because only 1% superconducting volume fraction has been observed in the material.

(2) Regarding the 4310 phase, recent high-pressure studies on their pure phases found that its superconductivity exhibits at around 20 K but at significantly higher pressure than that observed in $\text{La}_3\text{Ni}_2\text{O}_7$ ^{29,48,67-69}. These results suggest that the superconductivity with near 80 K observed in $\text{La}_3\text{Ni}_2\text{O}_7$ does not develop from the pure 4310 phase.

(3) Since the mixture of the 327 and 214 phases was absence of superconductivity under pressure⁷⁰, its contribution to the superconductivity can be excluded.

(4) Based on our STEM investigations, neither the polycrystalline nor single crystal samples exhibited the presence of a polymorph with a 1313 stacking sequence. This absence may be attributed to the possibility that the amount of 1313 polymorph is too small to be found by STEM. Since we did not observe any 1313 phase in all our samples by STEM, this peculiar polymorph can be excluded to be associated with the observed superconductivity in $\text{La}_3\text{Ni}_2\text{O}_7$.

(5) Given that our single crystal sample comprises only the 327 and 4310 phases, which were also identified in the polycrystalline samples, we propose that the superconductivity with a 1% superconducting volume fraction is most likely originated from the interface between the 327 and 4310 phases.

(6) Through our investigations involving high-pressure resistance and modulated *ac* susceptibility measurements on polycrystalline samples, we know that the significantly increased specific surface area of the polycrystalline sample does not lead to an increase in the superconducting volume fraction, which implies that superconductivity in $\text{La}_3\text{Ni}_2\text{O}_7$ does not present on the crystal surface.

In conclusion, we are the first to confirm the existence of high-temperature superconductivity in $\text{La}_3\text{Ni}_2\text{O}_7$ through demonstrating both of zero resistance and diamagnetism, and subsequently quantify the superconducting volume fraction at the level of 1%. These findings provide vital insights in understanding the anomalous superconducting behavior of the compressed $\text{La}_3\text{Ni}_2\text{O}_7$. Furthermore, our

measurements of resistance and *ac* susceptibility consistently demonstrate the reversibility of pressure-induced superconductivity, indicating that the superconducting phase exists in a metastable state. Our STEM investigation on both of the $\text{La}_3\text{Ni}_2\text{O}_7$ single crystal and polycrystalline samples reveal that the observed filamentary superconductivity in this material most likely emerges at the interface between 327 and 4310 phases. If this is case, it is reasonable to anticipate that enhancing the interface between 327 and 4310 phases is a potential route for increasing the superconducting volume fraction⁷¹. Further, we have determined the upper and lower bounds of the oxygen content for the presence of superconductivity in the compressed $\text{La}_3\text{Ni}_2\text{O}_7$, approximately 7.35 and 6.89, respectively.

Our findings then raise significant questions that warrant further investigation, which include (1) Why does the coexistence between the 327 and 4310 phases possess the ability to develop the high- T_c superconductivity? (2) Is the valence change of Ni ions in the compressed $\text{La}_3\text{Ni}_2\text{O}_7$ related to its superconductivity? (3) Why the stoichiometric oxygen content is favorable for the presence of superconductivity? Addressing these questions may not only provide deeper insights into understanding the underlying physics for the superconductivity in this nickelates, as well as for the universal mechanism for high- T_c superconductivity, but also an effective guidance for exploring new high- T_c superconductors in *3d* transition metal compounds.

References

1. Sun, H., Huo, M., Hu, X., Li, J., Liu, Z., Han, Y., Tang, L., Mao, Z., Yang, P., Wang, B., Cheng,

- J., Yao, D.-X., Zhang, G.-M. & Wang, M. Signatures of superconductivity near 80 K in a nickelate under high pressure. *Nature* **621**, 493–498 (2023).
2. Wu, M. K., Ashburn, JR, Torng, C. J., Hor, P. H., Meng, R. L., Gao, L., Huang, Z. J., Wang, Y. Q. & Chu, C. W. Superconductivity at 93 K in a new mixed-phase Yb-Ba-Cu-O compound system at ambient pressure. *Phys. Rev. Lett.* **58**, 908–910 (1987).
 3. Bednorz, J. G. & Müller, K. A. Possible high T_C superconductivity in the Ba-La-Cu-O system. *Z. Physik B - Condensed Matter* **64**, 189–193 (1986).
 4. Kamihara, Y., Watanabe, T., Hirano, M. & Hosono, H. Iron-based layered superconductor $\text{LaO}_{(1-x)}\text{F}_{(x)}\text{FeAs}$ ($x = 0.05\text{--}0.12$) with $T_C = 26$ K. *J. Am. Chem. Soc.* **130**, 3296–3297 (2008).
 5. Anisimov, V. I., Bukhvalov, D. & Rice, T. M. Electronic structure of possible nickelate analogs to the cuprates. *Phys. Rev. B* **59**, 7901–7906 (1999).
 6. Hayward, M. A. Topochemical reactions of layered transition-metal oxides. *Semicond. Sci. Technol.* **29**, 64010 (2014).
 7. Li, D., Lee, K., Wang, B. Y., Osada, M., Crossley, S., Lee, H. R., Cui, Y., Hikita, Y. & Hwang, H. Y. Superconductivity in an infinite-layer nickelate. *Nature* **572**, 624–627 (2019).
 8. Wang, N. N., Yang, M. W., Yang, Z., Chen, K. Y., Zhang, H., Zhang, Q. H., Zhu, Z. H., Uwatoko, Y., Gu, L., Dong, X. L., Sun, J. P., Jin, K. J. & Cheng, J.-G. Pressure-induced monotonic enhancement of T_C to over 30 K in superconducting $\text{Pr}_{0.82}\text{Sr}_{0.18}\text{NiO}_2$ thin films. *Nat. Commun.* **13**, 4367 (2022).
 9. Pan, G. A., Ferenc Segedin, D., LaBollita, H., Song, Q., Nica, E. M., Goodge, B. H., Pierce, A. T., Doyle, S., Novakov, S., Córdova Carrizales, D., N'Diaye, A. T., Shafer, P., Paik, H., Heron, J. T., Mason, J. A., Yacoby, A., Kourkoutis, L. F., Erten, O., Brooks, C. M., Botana, A. S. & Mundy, J. A. Superconductivity in a quintuple-layer square-planar nickelate. *Nat. Mater.* **21**, 160–164 (2022).
 10. Lee, K., Wang, B. Y., Osada, M., Goodge, B. H., Wang, T. C., Lee, Y., Harvey, S., Kim, W. J., Yu, Y., Murthy, C., Raghu, S., Kourkoutis, L. F. & Hwang, H. Y. Linear-in-temperature resistivity for optimally superconducting $(\text{Nd,Sr})\text{NiO}_2$. *Nature* **619**, 288–292 (2023).

11. Cao, Y. & Yang, Y. Flat bands promoted by Hund's rule coupling in the candidate double-layer high-temperature superconductor $\text{La}_3\text{Ni}_2\text{O}_7$ under high pressure. *Phys. Rev. B* **109**, L081105 (2024).
12. Jiang, K., Wang, Z. & Zhang, F.-C. High-Temperature Superconductivity in $\text{La}_3\text{Ni}_2\text{O}_7$. *Chinese Phys. Lett.* **41**, 17402 (2024).
13. Qu, X.-Z., Qu, D.-W., Chen, J., Wu, C., Yang, F., Li, W. & Su, G. Bilayer t-J-J \perp Model and Magnetically Mediated Pairing in the Pressurized Nickelate $\text{La}_3\text{Ni}_2\text{O}_7$. *Phys. Rev. Lett.* **132**, 36502 (2024).
14. Zhang, Y., Lin, L.-F., Moreo, A., Maier, T. A. & Dagotto, E. Electronic structure, magnetic correlations, and superconducting pairing in the reduced Ruddlesden-Popper bilayer $\text{La}_3\text{Ni}_2\text{O}_6$ under pressure: Different role of d orbital compared with $\text{La}_3\text{Ni}_2\text{O}_7$. *Phys. Rev. B* **109**, 45151 (2024).
15. Chen, X., Jiang, P., Li, J., Zhong, Z. & Lu, Y. Critical charge and spin instabilities in superconducting $\text{La}_3\text{Ni}_2\text{O}_7$. *arXiv.2307.07154* (2023).
16. Christiansson, V., Petocchi, F. & Werner, P. Correlated Electronic Structure of $\text{La}_3\text{Ni}_2\text{O}_7$ under Pressure. *Phys. Rev. Lett.* **131**, 206501 (2023).
17. Gu, Y., Le, C., Yang, Z., Wu, X. & Hu, J. Effective model and pairing tendency in bilayer Ni-based superconductor $\text{La}_3\text{Ni}_2\text{O}_7$. *arXiv.2306.07275* (2023).
18. Jiang, R., Hou, J., Fan, Z., Lang, Z.-J. & Ku, W. Pressure Driven Fractionalization of Ionic Spins Results in Cupratelike High- T_c Superconductivity in $\text{La}_3\text{Ni}_2\text{O}_7$. *Phys. Rev. Lett.* **132** (2024).
19. LaBollita, H., Pardo, V., Norman, M. R. & Botana, A. S. Electronic structure and magnetic properties of $\text{La}_3\text{Ni}_2\text{O}_7$ under pressure. *arXiv.2309.17279* (2023).
20. Lechermann, F., Gondolf, J., Bötzel, S. & Eremin, I. M. Electronic correlations and superconducting instability in $\text{La}_3\text{Ni}_2\text{O}_7$ under high pressure. *Phys. Rev. B* **108**, L201121 (2023).
21. Liao, Z., Chen, L., Duan, G., Wang, Y., Liu, C., Yu, R. & Si, Q. Electron correlations and superconductivity in $\text{La}_3\text{Ni}_2\text{O}_7$ under pressure tuning. *Phys. Rev. B* **108**, 214522 (2023).
22. Liu, Y.-B., Mei, J.-W., Ye, F., Chen, W.-Q. & Yang, F. s^\pm -Wave Pairing and the Destructive Role

- of Apical-Oxygen Deficiencies in $\text{La}_3\text{Ni}_2\text{O}_7$ under Pressure. *Phys. Rev. Lett.* **131**, 236002 (2023).
23. Lu, C., Pan, Z., Yang, F. & Wu, C. Interlayer Coupling Driven High-Temperature Superconductivity in $\text{La}_3\text{Ni}_2\text{O}_7$ Under Pressure. *arXiv.2307.14965* (2023).
24. Lu, D.-C., Li, M., Zeng, Z.-Y., Hou, W., Wang, J., Yang, F. & You, Y.-Z. Superconductivity from Doping Symmetric Mass Generation Insulators: Application to $\text{La}_3\text{Ni}_2\text{O}_7$ under Pressure. *arXiv.2308.11195* (2023).
25. Luo, Z., Hu, X., Wang, M., Wú, W. & Yao, D.-X. Bilayer Two-Orbital Model of $\text{La}_3\text{Ni}_2\text{O}_7$ under Pressure. *Phys. Rev. Lett.* **131**, 126001 (2023).
26. Oh, H. & Zhang, Y.-H. Type-II t–J model and shared superexchange coupling from Hund’s rule in superconducting $\text{La}_3\text{Ni}_2\text{O}_7$. *Phys. Rev. B* **108**, 174511 (2023).
27. Qin, Q. & Yang, Y. High- T_C superconductivity by mobilizing local spin singlets and possible route to higher T_C in pressurized $\text{La}_3\text{Ni}_2\text{O}_7$. *Phys. Rev. B* **108**, L140504 (2023).
28. Sakakibara, H., Kitamine, N., Ochi, M. & Kuroki, K. Possible high T_C superconductivity in $\text{La}_3\text{Ni}_2\text{O}_7$ under high pressure through manifestation of a nearly-half-filled bilayer Hubbard model. *arXiv.2306.06039* (2023).
29. Sakakibara, H., Ochi, M., Nagata, H., Ueki, Y., Sakurai, H., Matsumoto, R., Terashima, K., Hirose, K., Ohta, H., Kato, M., Takano, Y. & Kuroki, K. Theoretical analysis on the possibility of superconductivity in a trilayer Ruddlesden-Popper nickelate $\text{La}_4\text{Ni}_3\text{O}_{10}$ under pressure and its experimental examination: comparison with $\text{La}_3\text{Ni}_2\text{O}_7$. *arXiv.2309.09462* (2023).
30. Shilenko, D. A. & Leonov, I. V. Correlated electronic structure, orbital-selective behavior, and magnetic correlations in double-layer $\text{La}_3\text{Ni}_2\text{O}_7$ under pressure. *Phys. Rev. B* **108**, 125105 (2023).
31. Shen, Y., Qin, M. & Zhang, G.-M. Effective Bi-Layer Model Hamiltonian and Density-Matrix Renormalization Group Study for the High- T_C Superconductivity in $\text{La}_3\text{Ni}_2\text{O}_7$ under High Pressure. *Chinese Phys. Lett.* **40**, 127401 (2023).
32. Tian, Y.-H., Chen, Y., Wang, J.-M., He, R.-Q. & Lu, Z.-Y. Correlation Effects and Concomitant Two-Orbital s-Wave Superconductivity in $\text{La}_3\text{Ni}_2\text{O}_7$ under High Pressure. *arXiv.2308.09698*

(2023).

33. Wú, W., Luo, Z., Yao, D.-X. & Wang, M. Charge Transfer and Zhang-Rice Singlet Bands in the Nickelate Superconductor $\text{La}_3\text{Ni}_2\text{O}_7$ under Pressure. *arXiv.2307.05662* (2023).
34. Yang, Q.-G., Da Wang & Wang, Q.-H. Possible s_{\pm} -wave superconductivity in $\text{La}_3\text{Ni}_2\text{O}_7$. *Phys. Rev. B* **108**, L140505 (2023).
35. Yang, Y., Zhang, G.-M. & Zhang, F.-C. Minimal effective model and possible high- T_C mechanism for superconductivity of $\text{La}_3\text{Ni}_2\text{O}_7$ under high pressure. *arXiv.2308.01176* (2023).
36. Zhang, J.-X., Zhang, H.-K., You, Y.-Z. & Weng, Z.-Y. Strong Pairing Originated from an Emergent Z_2 Berry Phase in $\text{La}_3\text{Ni}_2\text{O}_7$. *arXiv.2309.05726* (2023).
37. Zhang, Y., Lin, L.-F., Moreo, A. & Dagotto, E. Electronic structure, dimer physics, orbital-selective behavior, and magnetic tendencies in the bilayer nickelate superconductor $\text{La}_3\text{Ni}_2\text{O}_7$ under pressure. *Phys. Rev. B* **108**, L180510 (2023).
38. Zhang, Y., Lin, L.-F., Moreo, A., Maier, T. A. & Dagotto, E. Structural phase transition, s_{\pm} -wave pairing, and magnetic stripe order in bilayered superconductor $\text{La}_3\text{Ni}_2\text{O}_7$ under pressure. *Nat. Commun.* **15**, 2470 (2024).
39. Zhang, Y., Lin, L.-F., Moreo, A., Maier, T. A. & Dagotto, E. Trends in electronic structures and s_{\pm} -wave pairing for the rare-earth series in bilayer nickelate superconductor $\text{R}_3\text{Ni}_2\text{O}_7$. *Phys. Rev. B* **108**, 165141 (2023).
40. Yang, J., Sun, H., Hu, X., Xie, Y., Miao, T., Luo, H., Chen, H., Liang, B., Zhu, W., Qu, G., Chen, C.-Q., Huo, M., Huang, Y., Zhang, S., Zhang, F., Yang, F., Wang, Z., Peng, Q., Mao, H., Liu, G., Xu, Z., Qian, T., Yao, D.-X., Wang, M., Zhao, L. & Zhou, X. J. Orbital-Dependent Electron Correlation in Double-Layer Nickelate $\text{La}_3\text{Ni}_2\text{O}_7$. *arXiv.2309.01148* (2023).
41. Abadi, S. N., Xu, K.-J., Lomeli, E. G., Puphal, P., Isobe, M., Zhong, Y., Fedorov, A. V., Mo, S.-K., Hashimoto, M., Lu, D.-H., Moritz, B., Keimer, B., Devereaux, T. P., Hepting, M. & Shen, Z.-X. Electronic structure of the alternating monolayer-trilayer phase of $\text{La}_3\text{Ni}_2\text{O}_7$. *arXiv.2402.07143* (2024).
42. Chen, X., Choi, J., Jiang, Z., Mei, J., Jiang, K., Li, J., Agrestini, S., Garcia-Fernandez, M.,

- Huang, X., Sun, H., Shen, D., Wang, M., Hu, J., Lu, Y., Zhou, K.-J. & Feng, D. Electronic and magnetic excitations in $\text{La}_3\text{Ni}_2\text{O}_7$. *arXiv.2401.12657* (2024).
43. Liu, Z., Huo, M., Li, J., Li, Q., Liu, Y., Dai, Y., Zhou, X., Hao, J., Lu, Y., Wang, M. & Wen, H. Electronic correlations and energy gap in the bilayer nickelate $\text{La}_3\text{Ni}_2\text{O}_7$. *arXiv.2307.02950* (2023).
44. Zhang, F. C. & Rice, T. M. Effective Hamiltonian for the superconducting Cu oxides. *Phys. Rev. B* **37**, 3759–3761 (1988).
45. Zhang, Y., Su, D., Huang, Y., Sun, H., Huo, M., Shan, Z., Ye, K., Yang, Z., Li, R., Smidman, M., Wang, M., Jiao, L. & Yuan, H. High-temperature superconductivity with zero-resistance and strange metal behavior in $\text{La}_3\text{Ni}_2\text{O}_7$. *arXiv.2307.14819* (2023).
46. Hou, J., Yang, P.-T., Liu, Z.-Y., Li, J.-Y., Shan, P.-F., Ma, L., Wang, G., Wang, N.-N., Guo, H.-Z., Sun, J.-P., Uwatoko, Y., Wang, M., Zhang, G.-M., Wang, B.-S. & Cheng, J.-G. Emergence of High-Temperature Superconducting Phase in Pressurized $\text{La}_3\text{Ni}_2\text{O}_7$ Crystals. *Chinese Phys. Lett.* **40**, 117302 (2023).
47. Wang, G., Wang, N. N., Shen, X. L., Hou, J., Ma, L., Shi, L. F., Ren, Z. A., Gu, Y. D., Ma, H. M., Yang, P. T., Liu, Z. Y., Guo, H. Z., Sun, J. P., Zhang, G. M., Calder, S., Yan, J.-Q., Wang, B. S., Uwatoko, Y. & Cheng, J.-G. Pressure-Induced Superconductivity In Polycrystalline $\text{La}_3\text{Ni}_2\text{O}_{7-\delta}$. *Phys. Rev. X* **14**, 11040 (2024).
48. Zhang, M., Pei, C., Wang, Q., Zhao, Y., Li, C., Cao, W., Zhu, S., Wu, J. & Qi, Y. Effects of pressure and doping on Ruddlesden-Popper phases $\text{La}_{n+1}\text{Ni}_n\text{O}_{3n+1}$. *Journal of Materials Science & Technology* **185**, 147–154 (2024).
49. Chen, X., Zhang, J., Thind, A. S., Sharma, S., LaBollita, H., Peterson, G., Zheng, H., Phelan, D. P., Botana, A. S., Klie, R. F. & Mitchell, J. F. Polymorphism in the Ruddlesden-Popper Nickelate $\text{La}_3\text{Ni}_2\text{O}_7$: Discovery of a Hidden Phase with Distinctive Layer Stacking. *J. Am. Chem. Soc.* **146**, 3640–3645 (2024).
50. Li, F., Guo, N., Zheng, Q., Shen, Y., Wang, S., Cui, Q., Liu, C., Wang, S., Tao, X., Zhang, G.-

- M. & Zhang, J. Design and synthesis of three-dimensional hybrid Ruddlesden-Popper nickelate single crystals. *arXiv.2312.08116* (2024).
51. Dong, Z., Huo, M., Li, J., Li, J., Li, P., Sun, H., Lu, Y., Wang, M., Wang, Y. & Chen, Z. Visualization of Oxygen Vacancies and Self-doped Ligand Holes in $\text{La}_3\text{Ni}_2\text{O}_{7-\delta}$. *arXiv.2312.15727* (2023).
52. Puphal, P., Reiss, P., Enderlein, N., Wu, Y.-M., Khaliullin, G., Sundaramurthy, V., Priessnitz, T., Knauff, M., Richter, L., Isobe, M., van Aken, P. A., Takagi, H., Keimer, B., Suyolcu, Y. E., Wehinger, B., Hansmann, P. & Hepting, M. Unconventional crystal structure of the high-pressure superconductor $\text{La}_3\text{Ni}_2\text{O}_7$. *arXiv.2312.07341* (2023).
53. Wang, H., Chen, L., Rutherford, A., Zhou, H. & Xie, W. Long-Range Structural Order in a Hidden Phase of Ruddlesden–Popper Bilayer Nickelate $\text{La}_3\text{Ni}_2\text{O}_7$. *Inorg. Chem.* **63**, 5020–5026 (2024).
54. Ishizuka, M., Iketani, M. & Endo, S. Pressure effect on superconductivity of vanadium at megabar pressures. *Phys. Rev. B* **61**, R3823–R3825 (2000).
55. Timofeev, Y. A., Struzhkin, V. V., Hemley, R. J., Mao, H. & Gregoryanz, E. A. Improved techniques for measurement of superconductivity in diamond anvil cells by magnetic susceptibility. *Rev. Sci. Instrum.* **73**, 371–377 (2002).
56. Timofeev, Y. A. & Utyuzh, A. N. Detection of Superconductivity in a High-Pressure Chamber with Diamond Anvils by Mutual Induction Method with Laser-Modulated Sample Temperature. *Instrum. Exp. Tech.* **48**, 550–555 (2005).
57. Mohn, P. *Magnetism in the solid state. An introduction*. 2nd ed. (Springer, Berlin, New York, 2006).
58. Wang, L., Li, Y., Xie, S.-Y., Liu, F., Sun, H., Huang, C., Gao, Y., Nakagawa, T., Fu, B., Dong, B., Cao, Z., Yu, R., Kawaguchi, S. I., Kadobayashi, H., Wang, M., Jin, C., Mao, H. & Liu, H. Structure Responsible for the Superconducting State in $\text{La}_3\text{Ni}_2\text{O}_7$ at High-Pressure and Low-Temperature Conditions. *J. Am. Chem. Soc.* (2024).
59. Gofryk, K., Pan, M., Cantoni, C., Sapiro, B., Mitchell, J. E. & Sefat, A. S. Local

- inhomogeneity and filamentary superconductivity in Pr-doped CaFe_2As_2 . *Phys. Rev. Lett.* **112**, 47005 (2014).
60. Saha, S. R., Butch, N. P., Kirshenbaum, K., Paglione, J. & Zavalij, P. Y. Superconducting and ferromagnetic phases induced by lattice distortions in stoichiometric SrFe_2As_2 single crystals. *Phys. Rev. Lett.* **103**, 37005 (2009).
61. Hsu, S. W., Tsaur, S. Y. & Ku, H. C. Effect of oxygen on the filamentary superconductivity of the $\text{La}_{2-x}\text{CuO}_{4-\delta}$ system. *Phys. Rev. B* **38**, 856–858 (1988).
62. Grenier, J.-C., Lagueyte, N., Wattiaux, A., Doumerc, J.-P., Dordor, P., Etourneau, J., Pouchard, M., Goodenough, J. B. & Zhou, J. S. Transport and magnetic properties of the superconducting $\text{La}_2\text{CuO}_{4+\delta}$ phases ($0 < \delta < 0.09$) prepared by electrochemical oxidation. *Physica C: Superconductivity* **202**, 209–218 (1992).
63. Grenier, J.-C., Wattiaux, A., Demourgues, A., Pouchard, M. & Hagenmuller, P. Electrochemical oxidation: a new way for preparing high oxidation states of transition metals. *Solid State Ionics* **63-65**, 825–832 (1993).
64. Gao, R., Jin, L., Huyan, S., Ni, D., Wang, H., Xu, X., Bud'ko, S. L., Canfield, P., Xie, W. & Cava, R. J. Is $\text{La}_3\text{Ni}_2\text{O}_{6.5}$ a Bulk Superconducting Nickelate? *ACS applied materials & interfaces* **3c**, 17376 (2024).
65. Demourgues, A., Weill, F., Darriet, B., Wattiaux, A., Grenier, J. C., Gravereau, P. & Pouchard, M. Additional Oxygen Ordering in “ $\text{La}_2\text{NiO}_{4.25}$ ” ($\text{La}_8\text{Ni}_4\text{O}_{17}$). *Journal of Solid State Chemistry* **106**, 317–329 (1993).
66. Carvalho, M. D., Wattiaux, A., Bassat, J. M., Grenier, J. C., Pouchard, M., Da Silva Pereira, M. I. & Costa, F. M. A. Electrochemical oxidation and reduction of $\text{La}_4\text{Ni}_3\text{O}_{10}$ in alkaline media. *J Solid State Electrochem* **7**, 700–705 (2003).
67. Zhu, Y., Zhang, E., Pan, B., Chen, X., Di Peng, Chen, L., Ren, H., Liu, F., Li, N., Xing, Z., Han, J., Wang, J., Jia, D., Wo, H., Gu, Y., Gu, Y., Ji, L., Wang, W., Gou, H., Shen, Y., Ying, T., Chen, X., Yang, W., Zheng, C., Zeng, Q., Guo, J.-G. & Zhao, J. Superconductivity in trilayer nickelate $\text{La}_4\text{Ni}_3\text{O}_{10}$ single crystals. *arXiv.2311.07353* (2023).

68. Zhang, M., Pei, C., Du, X., Cao, Y., Wang, Q., Wu, J., Li, Y., Zhao, Y., Li, C., Cao, W., Zhu, S., Zhang, Q., Yu, N., Cheng, P., Zhao, J., Chen, Y., Guo, H., Yang, L. & Qi, Y. Superconductivity in trilayer nickelate $\text{La}_4\text{Ni}_3\text{O}_{10}$ under pressure. *arXiv.2311.07423* (2023).
69. Li, Q., Zhang, Y.-J., Xiang, Z.-N., Zhang, Y., Zhu, X. & Wen, H. Signature of Superconductivity in Pressurized $\text{La}_4\text{Ni}_3\text{O}_{10}$. *Chinese Phys. Lett.* **41**, 17401 (2024).
70. Private communication with Zhang, J.
71. Ran, F., Liang, Y. & Jiandi, Z. Quasi-two-dimensional superconductivity at oxide heterostructures. *Acta Phys. Sin.* **72**, 97401 (2023).

Acknowledgements

The work was supported by the National Key Research and Development Program of China (Grant No. 2022YFA1403900 and 2021YFA1401800), the NSF of China (Grant Numbers Grants No. U2032214, 12122414, 12104487 and 12004419) and the Strategic Priority Research Program (B) of the Chinese Academy of Sciences (Grant No. XDB25000000). J. G. is grateful for supports from the Youth Innovation Promotion Association of the CAS (2019008).

Author contributions

L.S., H.K.M., T.X. and Q.W. designed the study and supervised the project. H.L.S. provides the $\text{La}_3\text{Ni}_2\text{O}_7$ single crystals. Z.Y.Z. synthesized the $\text{La}_3\text{Ni}_2\text{O}_{7-\delta}$ and $\text{La}_3\text{Ni}_2\text{O}_{7+\delta}$ polycrystalline samples. Z.Y.Z. and S.C. performed high-pressure modulated *ac* susceptibility measurements, J.G., S.C., P.Y.W., J.Y.Z. and J.Y.H. performed the high-pressure resistance and Hall coefficient measurements. Z.Y.Z.

performed experiments of electrochemical reaction. S.C. conducted single crystal x-ray diffraction measurements for the ambient-pressure sample. Y.J.C. performed STEM investigations. L.S., T.X., Q.W., Y.D., H.K.M., Y.Z. Z., J. G. and S.C. analyzed data. L.S., H.K.M., T.X., Q.W., Y.Z.Y. and J.G. wrote the manuscript with the efforts of all authors.

Additional information

These authors with star (*) contributed equally to this work.

Correspondence and requests for materials should be addressed to Ho-kwang Mao (maohk@hpstar.ac.cn) and Liling Sun (llsun@iphy.ac.cn or liling.sun@hpstar.ac.cn)

Competing interests

The authors declare no competing interests.

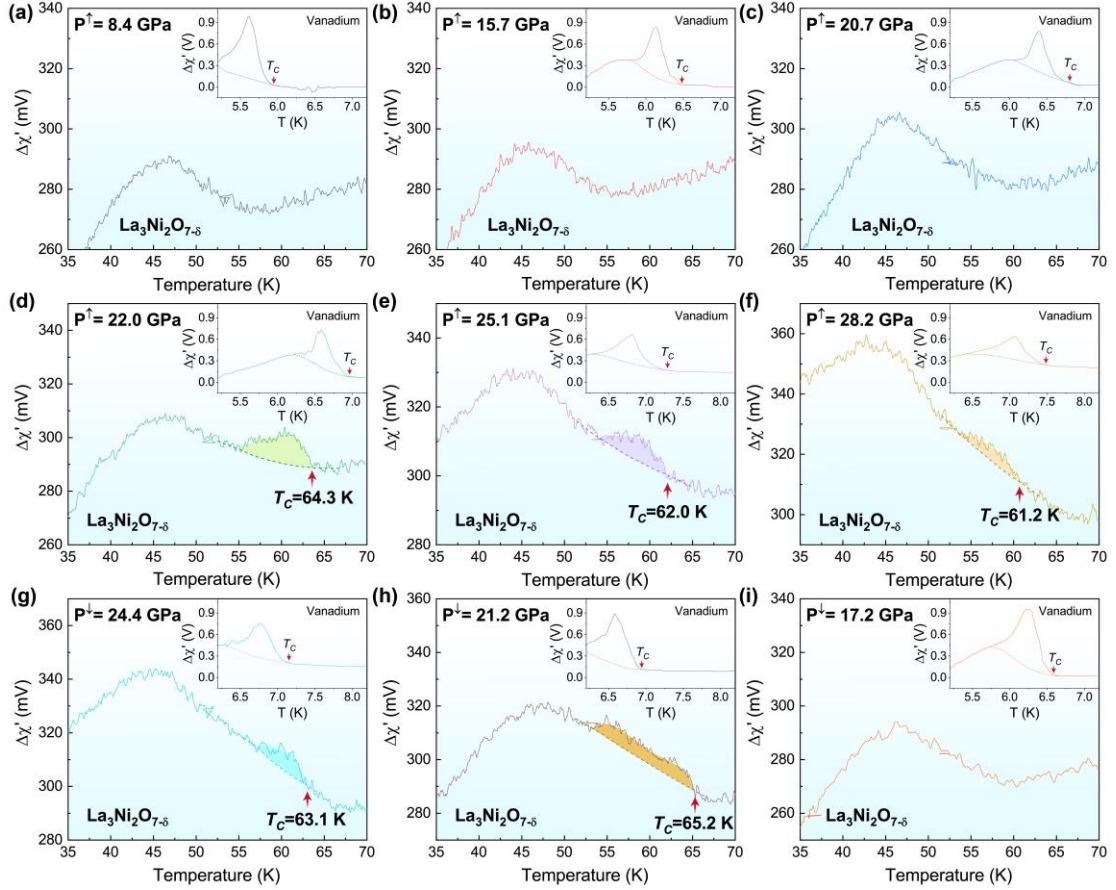


Figure 1 The raw data of the modulated ac susceptibility ($\Delta\chi'$) versus temperature (T) measured at different pressures for the $\text{La}_3\text{Ni}_2\text{O}_7$ single crystal. (a-c) The results obtained at 8.4, 15.7 and 20.7 GPa, respectively. Upon compression, no superconducting diamagnetic signal is observed. (d-f) The plots of $\Delta\chi'$ as a function of T measured at 22.0, 25.1 and 28.2 GPa, revealing a superconducting diamagnetic transition occurring at temperatures of 63.4, 62.0 and 61.2 K. (g-i) The data measured during the pressure releasing process, showing the loss of superconductivity at 17.2 GPa. The insets depict the corresponding superconducting transition of the elemental vanadium, captured through the synchronous measurements with the $\text{La}_3\text{Ni}_2\text{O}_7$ single crystal in the same high-pressure chamber. The onset T_c is indicated by the red arrow. By comparing the jump height of the sample and the vanadium, the superconducting

volume fraction of $\text{La}_3\text{Ni}_2\text{O}_7$ is estimated to be approximately 1% at 22.0 GPa, suggesting that the superconductivity of the compressed $\text{La}_3\text{Ni}_2\text{O}_7$ is filamentary-like.

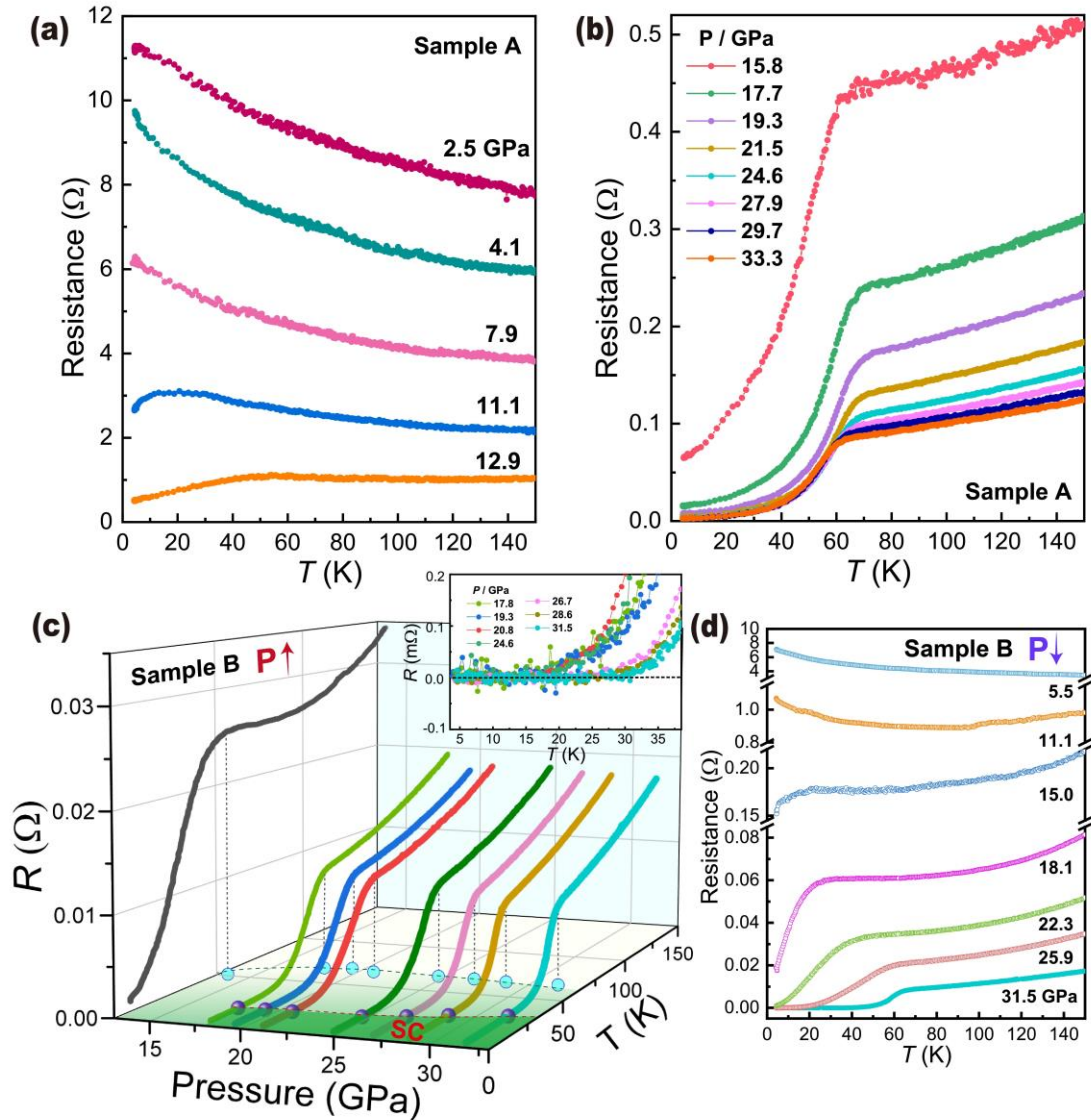


Figure 2 The temperature dependence of resistance measured at different pressures for the $\text{La}_2\text{Ni}_3\text{O}_7$ single crystals. (a-b) The results of resistance measurements on sample A within the pressure range of 2.5-33.3 GPa, illustrating the evolution from a semiconducting-like state to a superconducting-like state. (c) Resistance-temperature curves at different pressures for sample B, showing a

superconducting transition with zero resistance in the pressure range of 17.8-31.5 GPa.

The upper right panel displays an enlarged view of the low-temperature resistance. (d)

The results obtained from the pressure release measurements, demonstrating a gradual disruption of the superconducting state.

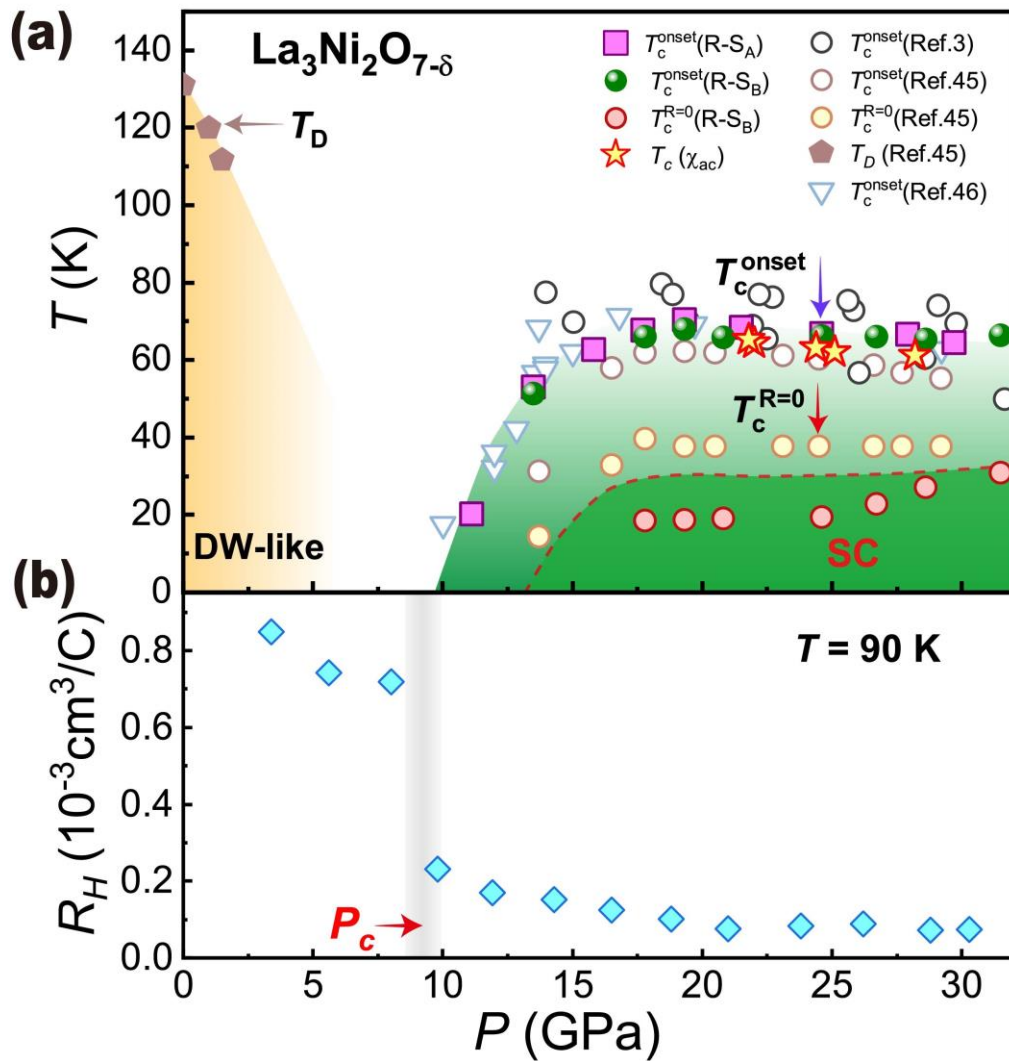


Figure 3 The pressure-temperature phase diagram and Hall coefficient (R_H) as a function of pressure for the $\text{La}_3\text{Ni}_2\text{O}_7$ single crystal. (a) A summary of our results and the reported results obtained from high-pressure modulated ac susceptibility and resistance measurements. The filled stars represent the data from our susceptibility

measurements. The green balls, squares and circles filled with pink are the data from our resistance measurements. DW and SC stand for density-wave and superconducting phases, respectively. T_D denotes the onset temperature of the DW-like phase transition, while T_c^{onset} and $T_c^{R=0}$ represent the onset and zero resistance temperature of the superconducting transition, respectively. (b) The plot of pressure versus Hall coefficient (R_H) measured at 90 K, demonstrating a significant drop in R_H around the boundary between the DW-like phase and the SC phase.

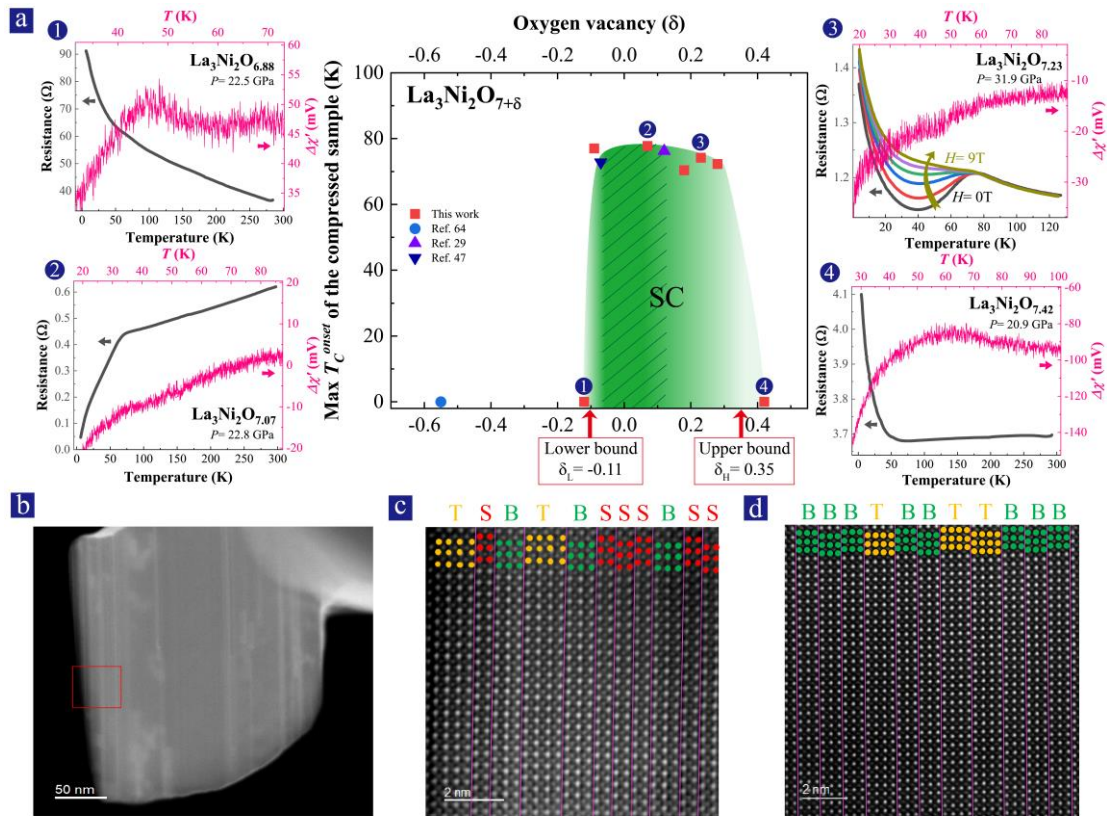


Figure 4 The lower and upper bounds of the oxygen vacancy for the presence of superconductivity and the images of STEM for the superconducting samples. (a) The connection of the oxygen vacancy in $\text{La}_3\text{Ni}_2\text{O}_{7+\delta}$ with the presence of superconductivity. The lower and upper bounds of the oxygen vacancy for the presence

of superconductivity are estimated to be about -0.11 and 0.35 respectively, the value of which is taken by an average of oxygen content for non-superconducting and superconducting samples ($\delta_L = [(7-6.88)+(7-6.91)]/2=0.11$, $\delta_H = [(7.42-7)+(7.28-7)]/2=0.35$). To visualize these findings, we have provided detailed results as labeled by 1, 2, 3, and 4 on the left and the right of main figure, which show the temperature-resistance and temperature-susceptibility results measured from the samples with different oxygen contents. The shaded region represents the range where the low temperature resistance of the sample exhibits metallic behavior, while outside of this region, the low temperature resistance of the sample displays a noticeable upturn. The modulated *ac* susceptibility measurements for sample #1 and sample #4 were conducted in Diamond Anvil Cell #1, resulting in both samples exhibiting the same background signal. Whereas the susceptibility measurements for sample #2 and sample #3 were performed in Diamond Anvil Cell #2, leading to both samples displaying the same background signal. (b) Low magnification low-angle annular dark-field (LAADF) scanning transmission electron microscopy (STEM) image along the [110] direction of the $\text{La}_3\text{Ni}_2\text{O}_{7.07}$ polycrystalline sample. The extensive gray regions correspond to the 327 phase with a 2222-stacking sequence, while the white line regions indicate the interface structure. (c) An atomic-scale high-angle annular dark-field (HAADF) image along the [110] direction obtained from the area within the red box in figure (b). This image reveals the layered stacking interface structure. (d) An atomic scale HAADF image along the [110] direction of the $\text{La}_3\text{Ni}_2\text{O}_7$ single crystal sample. In the images of (c) and (d), the atoms of La in the 327, 4310, and 124 phases are represented by orange,

red, and green dots, respectively. T, B, and S denote the trilayer, bilayer, and single-layer arrangements of Ni-O planes.